Transduction channels' gating can control friction on vibrating hair-cell bundles in the ear

Volker Bormuth[a,b,c], Jérémie Barral[a,b,c,1], Jean-François Joanny[a,b,c,d], Frank Jülicher[e], and Pascal Martin[a,b,c,2]

[a]Laboratoire Physico-Chimie Curie, Centre National de la Recherche Scientifique, Unité Mixte de Recherche 168, F-75248 Paris, France; [b]Institut Curie, Centre de recherche, F-75248 Paris, France; [c]Université Pierre et Marie Curie, F-75252 Paris, France; [d]École Supérieure de Physique et de Chimie Industrielles Paris Tech, F-75231 Paris, France; and [e]Max Planck Institute for the Physics of Complex Systems, D-01187 Dresden, Germany

Edited by David A. Weitz, Harvard University, Cambridge, MA, and approved April 8, 2014 (received for review February 12, 2014)

Hearing starts when sound-evoked mechanical vibrations of the hair-cell bundle activate mechanosensitive ion channels, giving birth to an electrical signal. As for any mechanical system, friction impedes movements of the hair bundle and thus constrains the sensitivity and frequency selectivity of auditory transduction. Friction is generally thought to result mainly from viscous drag by the surrounding fluid. We demonstrate here that the opening and closing of the transduction channels produce internal frictional forces that can dominate viscous drag on the micrometer-sized hair bundle. We characterized friction by analyzing hysteresis in the force–displacement relation of single hair-cell bundles in response to periodic triangular stimuli. For bundle velocities high enough to outrun adaptation, we found that frictional forces were maximal within the narrow region of deflections that elicited significant channel gating, plummeted upon application of a channel blocker, and displayed a sublinear growth for increasing bundle velocity. At low velocity, the slope of the relation between the frictional force and velocity was nearly fivefold larger than the hydrodynamic friction coefficient that was measured when the transduction machinery was decoupled from bundle motion by severing tip links. A theoretical analysis reveals that channel friction arises from coupling the dynamics of the conformational change associated with channel gating to tip-link tension. Varying channel properties affects friction, with faster channels producing smaller friction. We propose that this intrinsic source of friction may contribute to the process that sets the hair cell's characteristic frequency of responsiveness.

mechanosensitive channels | protein friction | hair-bundle mechanosensitivity | cell mechanics | auditory system

Sound evokes vibrations in the inner ear that are detected by sensory hair cells. Mechanosensitivity stems from mechanical activation of ion channels by tension changes in tip links that interconnect neighboring stereocilia of the hair-cell bundle (1). The acute sensitivity and sharp frequency selectivity of auditory detection rely on efficient transmission of the energy derived from the acoustic stimulus to the apparatus that mediates mechanoelectrical transduction. However, at least three sources of friction threaten to dissipate the energy of the vibrating hair bundle. First, viscous drag by the surrounding fluid provides a minimum source of damping (2, 3). Second, viscoelasticity of the tip links, or of proteins in series with these links, may result in additional dissipation during hair-bundle deflections (4). Third, an intrinsic source of friction—called "channel friction" in the following—is related to thermal fluctuations of the transduction channels between their open and closed states (5). The fluctuation–dissipation theorem dictates that this source of mechanical noise be related to friction forces on the hair bundle.

To circumvent the fundamental challenge posed by friction, hair cells mobilize internal energy resources to produce mechanical work, negate friction, and in turn amplify its inputs at a characteristic frequency (6, 7). In particular, the hair cell can power active movements of its hair bundle, including spontaneous oscillations (8, 9). Nevertheless, the performance of the hair bundle, both as transducer and amplifier, are influenced by friction for two reasons. First, friction limits the sensitivity of the hair bundle to weak inputs (5, 10). Second, the strength and dynamics of active force production must be tuned to balance friction that impedes movements of a particular bundle at its characteristic frequency (11). Despite their key role in hair-cell mechanosensitivity, the various sources of friction acting on a moving hair bundle, and how they depend on bundle velocity, have not been assayed directly through force measurements.

In this work, we combine a dynamic force assay with pharmacological tools to decipher the relative contributions of viscous drag, tip-link viscoelasticity, and channel friction to hair-bundle friction. By using a channel blocker to test the implication of transduction channels' gating, we unveil the contribution of channel friction. By disrupting the tip links, we decouple the transduction apparatus from bundle motion and measure viscous drag on the hair-bundle structure. We find that channel friction can dominate viscous drag. We also vary bundle velocity both to study the dynamical properties of friction and to determine how active hair-bundle motility affects friction estimates. We interpret our observations by developing a physical description of active hair-bundle mechanics and explain the mechanism of channel friction.

Results

To probe friction, we used flexible glass fibers to apply periodic stimuli to single hair-cell bundles from an excised preparation of the bullfrog's saccule (Fig. 1; *Materials and Methods*). Under natural ionic conditions, the hair bundles displayed spontaneous oscillations at frequencies of 5–80 Hz (12). We monitored the

Significance

In this work, we developed a dynamic force assay to characterize frictional forces that impede sound-evoked vibrations of hair-cell bundles, the mechanosensory antennas of the inner ear. We find that opening and closing of mechanosensitive ion channels in the hair bundle produce frictional forces that can dominate viscous drag on the hair-bundle structure. We show that channel friction can be understood quantitatively using a physical theory of hair-bundle mechanics that includes channel kinetics. Friction originating from gating of ion channels is a concept that is relevant to all mechanosensitive channels. In the context of hearing, this channel friction may contribute to setting the characteristic frequency of the hair cell.

Author contributions: V.B., J.B., J.-F.J., F.J., and P.M. designed research, performed research, analyzed data, and wrote the paper.

The authors declare no conflict of interest.

This article is a PNAS Direct Submission.

Freely available online through the PNAS open access option.

[1]Present address: Center for Neural Science, New York University, New York, NY 10003.

[2]To whom correspondence should be addressed. E-mail: pascal.martin@curie.fr.

This article contains supporting information online at www.pnas.org/lookup/suppl/doi:10.1073/pnas.1402556111/-/DCSupplemental.

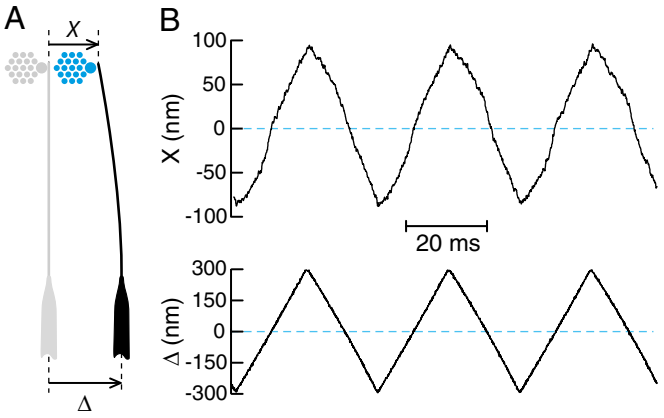

Fig. 1. Periodic triangular stimulation of a hair bundle. (*A*) Schematic top view of the experiment. The tip of a flexible fiber (black) is attached to the top of a hair bundle (blue). (*B*) Hair-bundle deflection *X* as a function of time (*Top*) in response to three cycles of a symmetric triangular movement Δ of the fiber's base (*Bottom*). Each positive or negative ramp of base motion had here a velocity of 34 μm·s^{-1}; the bundle was subjected to a total of 71 cycles. The fiber had a stiffness $k = 295$ μN·m^{-1} and a drag coefficient $\lambda = 113.4$ nN·s·m^{-1}.

time-dependent position $X(t)$ of the fiber's tip, and thus of the attached hair bundle, in response to a symmetric triangular waveform of motion of the fiber's base. By convention, a movement of the hair bundle from negative to positive deflections increased tip-link tension and thus promoted channel opening. This positive half-cycle of stimulation was followed by a movement of opposite directionality that favored channel closure and completed the cycle. Because we fully characterized the mechanical and dynamical properties of the stimulus fiber (*SI Appendix*, section 2), we could compute, at each instant *t*, the force $F(t)$ that was applied by the fiber to the bundle. At each bundle position, the force exerted during the positive half-cycle of stimulation differed from that measured on the way back, causing hysteresis in the force–displacement relation (Fig. 2*A*).

Clockwise circulation around the hysteretic cycle reflects energy dissipation. We characterized the underlying frictional force by measuring the half-height of the hysteretic cycle

$$\Phi(X) = [F^{+}(X) - F^{-}(X)]/2 \qquad [1]$$

as a function of position. Here and in the following, signs in the superscripts indicate the directionality of bundle motion. For a passive system, the force Φ represents the arithmetic mean of the absolute frictional force on the positive and negative half-cycles at the same position *X* (*SI Appendix*, section 3). We note that active force production by the hair bundle can affect the width of the hysteretic cycle and thus contribute to Φ. The contribution of the active process, however, ought to become negligible when the period of stimulation gets significantly shorter than that of spontaneous hair-bundle oscillation. Interestingly, the force $F^{+}(X)$ and $F^{-}(X)$ displayed inversion symmetry with respect to a specific reference point at position $X_0 \cong 0$ (*SI Appendix*, Fig. S1). As a result, for stimuli faster than the internal active process, the force $\Phi(X = X_0)$ represents the true frictional force at this position.

The friction estimate Φ depended on bundle position (Fig. 2*B*, black curve). The relation $\Phi(X)$ was bell-shaped, with a peak centered near the position of inversion symmetry of the hysteretic cycle. Bundle velocity also varied with bundle position (Fig. 1*B* and *SI Appendix*, Fig. S2). On each half-cycle, this property was associated with a nonlinear region of reduced slope in the force–displacement relation, indicating that the hair bundle became transiently softer as it traversed this region (Fig. 2 *A* and *C*). Correspondingly, the bundle moved at increased velocity at these positions. However, a peak prevailed (Fig. 2*D*) when the frictional force was divided, at each position, by the average local velocity of the hair bundle (*SI Appendix*, Fig. S2). Hence, hair-bundle friction cannot be explained by viscous drag on a rigid object moving through the fluid.

Notably, friction peaked within the range of positions that spanned the regions of reduced slope of the force–displacement cycle. We recognized in hair-bundle softening the phenomenon of gating compliance (13), which here betrayed opening or closing of the mechanosensory channels that mediate mechanoelectrical transduction. In addition, the friction peak was associated with a shift—hereafter called the gating shift—between the positions of maximal gating compliance (Fig. 2 *A* and *C*): the channels opened at a position of the hair bundle that was more positive on the positive half-cycle than that at which they reclosed on the way back. These observations suggest that gating of the transduction channels was involved in the production of frictional forces.

To test this hypothesis, we used iontophoresis to apply gentamicin, an aminoglycoside antibiotic that blocks the transduction channels. As expected from complete blockage of the channels, there was no sign of gating compliance in the force–displacement relation (Fig. 2 *A* and *C*, red curve). Strikingly, the friction peak collapsed upon application of the drug (Fig. 2 *B* and *D*). The hysteretic cycle exhibited a nearly uniform width close to that

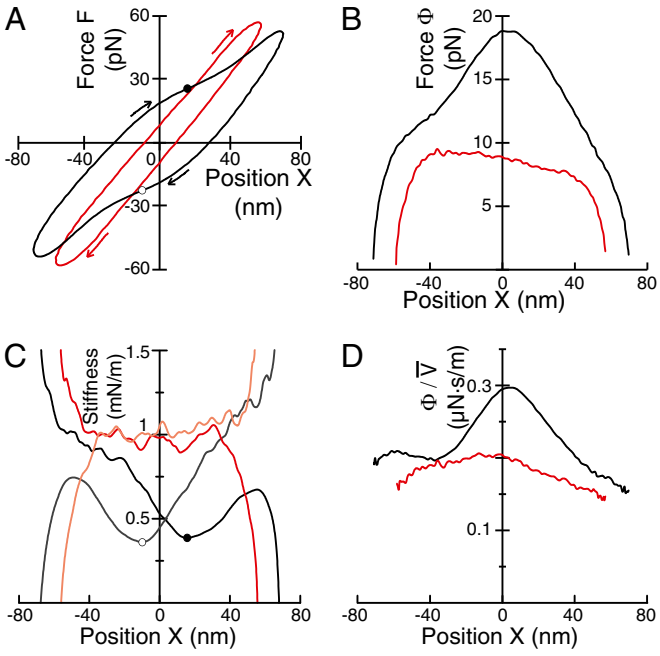

Fig. 2. Effects of a channel blocker on friction and stiffness. Black and red colors correspond, respectively, to measurements under control conditions and in the presence of a channel blocker. (*A*) External force *F* as a function of bundle position *X*. Arrows indicate clockwise circulation around a hysteretic cycle. The positions of minimal slope on the positive and negative half-cycles (black and white disk, respectively) are shifted by ΔX = +26 nm. (*B*) Vertical half-height Φ of the hysteretic cycles shown in *A* as a function of bundle position *X*. (*C*) Hair-bundle stiffness, measured as the local slope of the curves shown in *A*, as a function of bundle position *X* for positive (dark colors) and negative (light colors) half-cycles of stimulation. (*D*) At each position *X*, the force Φ shown in *B* was divided by the arithmetic mean $\overline{V} = [|V^{+}(X)| + |V^{-}(X)|]/2$ of the absolute velocities that the hair bundle assumed on the positive and negative half-cycles when crossing this position. The ratio $\Phi/\overline{V}$ is plotted as a function of *X*. The velocity of the fiber's base was fixed at 200 μm·s^{-1}; the hair bundle moved at a velocity $\overline{V} = 68$ μm·s^{-1}.

measured at large deflections under control conditions. We conclude that gating of the transduction channels evokes frictional forces on the hair bundle.

We then varied the velocity of stimulation. At low velocity of the fiber's base, we observed a counterclockwise circulation around the force–displacement cycle (*SI Appendix*, Fig. S3). This behavior reflects the work performed by an active process to power spontaneous oscillations of the hair bundle (14). Increasing the velocity switched the polarity of the hysteresis cycle, resulting in net positive dissipation (Fig. 3). We observed a dilation of the cycle along the force axis, with a more pronounced effect within the regions of gating compliance (Fig. 3*A*). Correspondingly, we measured negative frictional forces at low velocity, and a positive peak of friction emerged in response to increasing stimulus velocity (Fig. 3*B*).

If hydrodynamic drag were the dominant source of dissipation, we would expect friction to grow in proportion to velocity. A proportional growth was observed when the transduction machinery was decoupled from bundle motion by severing the tip links (Fig. 3*C* and *SI Appendix*, Fig. S4). Under this condition, the slope of the force–velocity relation provided a friction coefficient $\lambda_H = 86 \pm 29$ nN·s·m^{-1} (mean ± SD; $n = 10$). This value agrees with an estimate of the hydrodynamic drag coefficient of the hair bundle that resulted from finite-element simulations of the detailed interaction between the stereovillar structure and the fluid (2). Thus, friction on a bundle with severed tip links appears to be set by viscous drag.

With a fully functional transduction machinery, friction at the peak of the relation $\Phi(X)$ (Fig. 3*B*) displayed a sublinear growth with velocity (Fig. 3*C*). This behavior contrasts with the linear increase expected for hydrodynamic friction. At velocities larger than ~20 μm·s^{-1}, friction on the intact bundle was larger than that measured with broken tip links. The hair bundle thus appeared to be subjected to an intrinsic source of friction that adds to viscous drag. We then estimated friction within the shoulders of the friction peak (Fig. 3 *B* and *C*). After a steep rise at low velocities, friction matched that observed when the channels were blocked. This congruence makes sense because the stimulus ought to elicit no significant channel gating at the edges of the hysteretic cycle, where the channels are expected to be either mostly closed or open. As velocity increased, the two force–velocity relations approached the linear relation that was measured with severed tip links. However, friction was larger with channels blocked than with severed tip links, indicating that viscous drag was supplemented by additional friction even in the case where the channels were unable to gate.

Finally, we observed that the gating shift increased with bundle velocity (Fig. 3 *A* and *D*). This property reveals that the larger the velocity of motion, the further that bundle had to move in each direction before the transduction channels would actually gate. For velocities larger than ~30 μm·s^{-1}, the gating shift increased approximately in proportion to velocity. The slope of this relation provides twice the time of channel gating, which, at these velocities, is $\tau_{exp} = 230 \pm 40$ μs (mean ± SD; $n = 5$). This value lies within the range of the activation time constants of the transduction currents that were measured with the same type of hair cells (15). We reasoned that when the bundle moves, extra elastic energy is stored in the gating springs during the typical time τ_{exp} before the channels gate. Upon channel gating, this extra energy should be dissipated, giving rise to friction (16). In turn, we hypothesized that the friction peak that we observed in our recordings (Fig. 3*B*) may constitute the mechanical signature of delayed channel gating.

To test this inference, we introduced finite activation kinetics of the transduction channels into a physical description of active hair-bundle mechanics (17). First ignoring viscous drag and the active process, we studied the consequences of delayed gating for a passive bundle (*SI Appendix*, section 4). In response to triangular stimulation, the force–displacement relation shows hysteresis (Fig. 4*A*). Although no explicit source of dissipation was included in the description, we find that the system is subjected to frictional forces. Thus, delayed channel gating produces friction. As in our experiments (Fig. 2*B*), the mean frictional force Φ depends on position and displays a maximum (Fig. 4*B*). The theory indicates that this force is maximal at the position where the channels are half-open at steady state. When estimated at the peak, channel friction displays a sublinear growth as a function of velocity until it saturates to $\Phi_{max} = NZ/2$ at large velocities. Here N is the number of transduction channels operating in parallel within a hair bundle, and Z—the gating force (13)—represents the reduction in tip-link tension upon the conformational change associated with channel opening. At low velocities, the frictional force varies in proportion to velocity with a friction coefficient

$$\lambda_C = NZ^2\tau/(4k_BT). \quad [2]$$

Its value depends on the characteristic timescale τ of channel activation. Channel friction vanishes with instantaneous channel gating ($\tau \to 0$). In addition, channel-gating kinetics introduces a shift between the positions of channel opening and closing within the stimulation cycle. Simulations indicate that τ can be obtained from half the initial slope of the relation between the gating shift and velocity (Fig. 4*F*). With parameters listed in *SI Appendix*, Table S1, we find $\lambda_C = 1$ μN·s·m$^{-1} \cong 10 \times \lambda_H$. These values indicate that friction owing to gating of the transduction channels can indeed be strong enough to dominate viscous drag on the hair-bundle structure.

Because the hair bundle displays active motility (*SI Appendix*, Fig. S3), the force Φ is expected to depart from the passive friction estimate discussed in the preceding paragraph. To determine

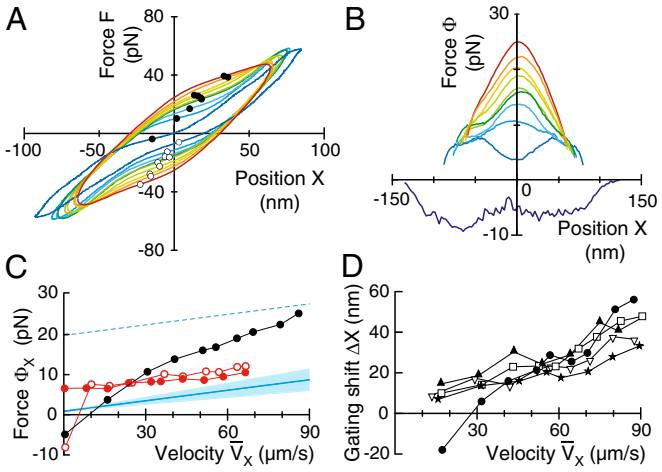

Fig. 3. Effects of stimulus velocity. (*A*) Force–displacement relations for increasing velocities of triangular stimulation (blue to red; cycle at lowest velocity shown in *SI Appendix*, Fig. S3). Positions of maximal gating compliance are marked by black and white disks (positive and negative half-cycle, respectively). (*B*) Friction estimate Φ as a function of bundle position *X*. (*C*) Under control conditions (same data as in *A* and *B*), the force Φ at $X = 3.5$ nm (black disks) or at $X = -52$ nm (red circles), noted Φ_X, is plotted as a function of the mean bundle velocity at this position, $\overline{V}_X$. Friction was also estimated in the presence of a channel blocker (red disks; same cell) and after severing the tip links (cyan solid line: mean behavior of 10 other cells; edges of the shaded region: SDs to the mean slope). The dashed line (same slope as the cyan solid line) serves as a guideline for the asymptotic behavior expected for the relation $\Phi_X(\overline{V}_X)$ under control conditions (Fig. 4*E*). (*D*) Gating shift ΔX as a function of velocity $\overline{V}_X$ at the peak of $\Phi(X)$ for five different cells, including that used in *A*–*C* (black disks).

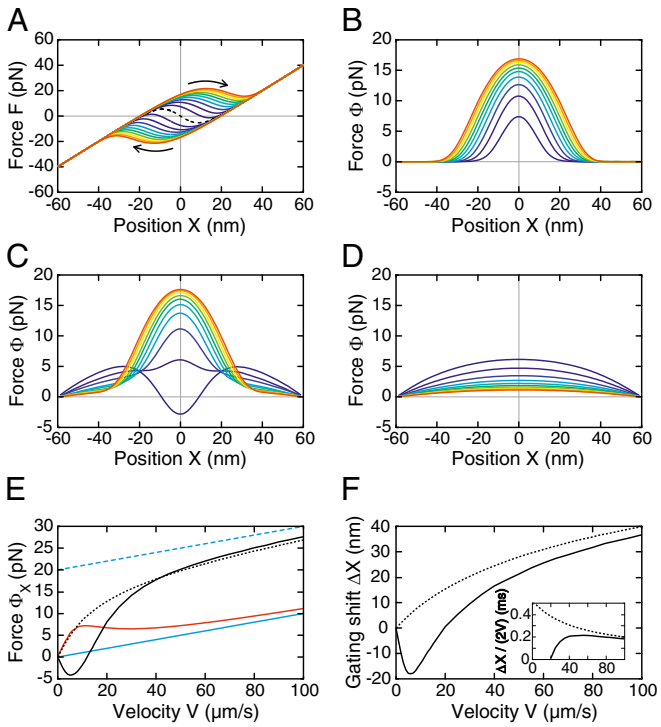

Fig. 4. Simulations of hair-bundle mechanics. The hair bundle follows triangular waveforms of motion. In *A*–*D*, viscous drag is ignored; bundle velocity V increases from 10 μm·s^{-1} (dark blue) to 100 μm·s^{-1} (red) in nine 10-μm·s^{-1} steps. (*A*) Force–displacement cycles $F(X)$ for a passive bundle (no adaptation). Arrows indicate clockwise circulation. With instantaneous channel gating, hysteresis vanishes (dashed line). (*B*) Channel-friction force Φ as a function of position X for the hysteretic cycles shown in *A*. (*C*) Relation $\Phi(X)$ with functional transduction channels and adaptation. (*D*) Relation $\Phi(X)$ resulting from adaptation when the channels are blocked. (*E*) Force Φ at $X = 0$, noted Φ_X, as a function of bundle velocity V when dissipation comes from viscous drag only (cyan solid), from channel friction and viscous drag (black dotted), from channel friction, viscous drag and adaptation (black solid), and from viscous drag and adaptation when the channels are blocked (red). At larges velocities, the relation $\Phi_X(V)$ (black solid and dotted) shows an asymptotic linear behavior (dashed cyan). (*F*) Gating shift ΔX, and estimate $\Delta X/(2V)$ of the channel activation time (*Inset*), as a function of bundle velocity V with or without adaptation (solid and dotted lines, respectively). Parameters in *SI Appendix*, Table S1.

how active hair-bundle motility affects Φ, we included calcium-dependent adaptation of the transduction apparatus (17) to our description (*SI Appendix*, section 5). At the edges of the stimulation cycle, where the channels are nearly all open or closed and thus do not add extra friction, or equivalently when the channels are blocked, adaptation produces in our simulations a positive contribution to the force Φ that leads to an overestimate of frictional forces (Fig. 4 *C*–*E*). This behavior may explain why the measured friction was larger with channels blocked than when the tip links were severed (Fig. 3*C*), although the tip links may by themselves be viscoelastic (4) or engage dissipative relative movements of adjacent stereocilia (18). In contrast, in the region of channel gating, the theory shows that frictional forces are underestimated at low bundle velocities, for the active process provides a negative contribution to Φ (Fig. 4 *C* and *E*). The effect of the active process can be neglected when the stimulus becomes fast enough to outrun adaptation but is significant at low velocities, where Φ can become negative (Fig. 4*E*). In the case where adaptation is functional (black solid line in Fig. 4*E*), we can construct a line of positive slope that starts from the origin and touches the force–velocity relation in one point. Its slope λ_0 provides a lower bound to the drag coefficient $\lambda_H + \lambda_C$ resulting from viscous drag and channel friction. In experiments (Fig. 3*C*), we measured a value $\lambda_0 = 425 \pm 70$ nN·s·m^{-1} (mean ± SD; $n = 6$), which was nearly fivefold the hydrodynamic drag coefficient λ_H. In addition, at velocities larger than 40 μm·s^{-1}, where the active process can be neglected, the slope of the relation between the gating shift and velocity (Figs. 3*D* and 4*F*) accounts for our measurement of the channel time $\tau_{exp} \cong 230$ μs (Fig. 4*F*, *Inset*).

Discussion

Physical Origin of Channel Friction. Our results demonstrate that gating of the transduction channels provides a major contribution to hair-bundle friction. It is striking that a few tens of ion channels (19, 20) can have a significant effect on friction of a structure as large as the micrometer-sized hair-cell bundle. If channel friction resulted simply from viscous drag associated with conformational changes of the channels moving in a fluid, we would estimate a friction coefficient ξ_H that is nearly four orders of magnitude lower than the value $\lambda_C \cong 340$ nN·s·m^{-1} measured here at low bundle velocity (*SI Appendix*, section 4).

Our physical description of hair-bundle mechanics attributes high channel friction to an intrinsic source of dissipation associated with channel gating (Fig. 4 and *SI Appendix*, section 4). In a simplified view, this can be explained by introducing an energy barrier E_a between two conformations of a channel. The effective friction coefficient associated to channel gating can then be approximated by $\xi \times \exp[E_a/(k_BT)]$, where ξ represents a microscopic friction coefficient acting on the channels' gates (21). If we take for ξ the rough hydrodynamic estimate ξ_H given above, an energy barrier $E_a \cong 10\ k_BT$ (15) brings channel friction to a level compatible with our experiments. Internal friction resulting from barrier crossing is thought to influence many processes in biology, including protein folding (22), protein–protein interactions (23, 24), cell adhesion (25), and the speed and efficiency of motor proteins (16, 26). Our work shows that this general concept of barrier friction also applies to mechanosensory ion channels and is thus relevant for the detection of sound-evoked vibrations by hair-cell bundles in the ear.

In the hair bundle, mechanosensitivity relies on strong coupling between the gating dynamics of the transduction channels and tip-link tension. If a change in tip-link tension affects the open probability of a transduction channel, then, reciprocally, channel gating must impinge on tip-link tension and thus produce force on the hair bundle (13, 27). However, it takes time to break the bonds that maintain an ion channel in a closed state. Channel-gating forces in turn lag the stimulus, which results in frictional resistance to hair-bundle movements and mechanical hysteresis. The effect of channel friction on the hair bundle is thus intimately related to the function of this organelle as a mechanoreceptor (*SI Appendix*, section 4).

Dual Role of Channel-Gating Forces. Sensitive mechanotransduction by hair cells calls for minimal frictional resistance to hair-bundle vibrations. However, our findings suggest that the hair bundle is not optimized to keep friction at the minimum level set by viscous drag on the hair-bundle structure. Weaker gating forces would reduce channel friction (Eq. 2 and *SI Appendix*, section 4). However, decreasing the magnitude of the gating force also broadens the sigmoidal relation between the channels' open probability and bundle displacement at thermal equilibrium (*SI Appendix*, section 4, Eq. S42) (28). Larger bundle displacements would in turn be required to elicit significant transduction currents, corresponding to lower mechanosensitivity of the transducer. Moreover, large gating forces also promote negative stiffness of the hair bundle, a property that has been shown to be instrumental in an active process that counteracts friction and in turn amplifies weak stimuli (29–31). Thus, gating forces may underlie both a prominent source of hair-bundle friction and

part of the solution to the general problem posed by friction to bundle mechanosensitivity.

Effect of Channel Friction on Characteristic Frequency. Frequency selectivity is a hallmark of active mechanosensation by hair cells. Several mechanisms have been implicated in the process that sets the characteristic frequency of optimal responsiveness, including electrical tuning of receptor potentials and passive mechanical resonance in a spring-mass system associated to accessory structures (32). Notably, spontaneous hair-bundle oscillations also provide a characteristic frequency near which the cell resonates with sinusoidal inputs, thus operating as an active filter (33). The active mechanical resonance occurs near the frequency of the periodic stimulus where active hair-bundle motility cancels friction (30, 34), which in our experiments happens at ∼10 Hz (Fig. 3*C*). This characteristic frequency is more than a hundred-fold smaller than the inverse of the channel activation time (>1 kHz). Consequently, the hair bundle operates in the low-frequency regime of channel friction, where this source of friction dominates viscous drag (Fig. 4 and *SI Appendix*, Fig. S10 in section 4). The characteristic frequency of the active resonator is expected to decrease with the frictional load (35, 36). The characteristic frequency should thus depend on the number of the transduction channels, the value of their gating force, and of their activation time (Eq. 2). In particular, faster channels ought to produce smaller channel friction, which would then allow faster hair-bundle movements. This property may be relevant to auditory organs where the activation kinetics of the transduction channels (37, 38), as well as the number and height of the stereocilia (39, 40), has been shown to vary systematically along a tonotopic axis. Varying channel properties, and in turn channel friction, could in principle help the hair cells set their characteristic frequency of maximal mechanical responsiveness over the broad range required for the analysis of complex natural sounds.

Auditory hair cells, in particular in the mammalian cochlea, are endowed with much faster channels than those of the low-frequency hair cells that we studied here in the bullfrog's sacculus. For instance, outer hair cells within the apical turn of the rat cochlea display activation channel times $\tau_{rat} \leq 50$ μs (37, 41). Although these cells respond to relatively high frequencies of ∼4 kHz, their characteristic frequency remains significantly smaller than the inverse of the channel time (>20 kHz). Auditory hair cells can thus operate in the low-frequency regime of channel friction. One may wonder whether channel friction is large enough to be relevant at auditory frequencies, for the magnitude of channel friction is expected to decrease with faster channels (Eq. 2). However, the number of channels that contribute to channel friction is larger for high-frequency than for low-frequency cells. In addition, the bundle height is smaller at high frequencies, which magnifies the effect of channel-gating forces (*SI Appendix*, section 4.3). Using scaling arguments, we estimate frictional forces from channel gating that may again be larger than those resulting from viscous drag (*SI Appendix*, section 4.3). Although experiments are needed to test this prediction, our results raise the possibility that channel friction may contribute to the complex process that sets the characteristic frequency of an auditory hair cell.

Materials and Methods

Experimental Preparation. Details of the experimental procedure have been published elsewhere (17). Briefly, an excised preparation of the bullfrog's (Rana catesbeiana) saccule was mounted on a two-compartment chamber. The basal bodies of hair cells were bathed in standard saline containing (in mM): 110 NaCl, 2 KCl, 4 $CaCl_2$, 3 D-glucose, 2 Na_2-creatine phosphate, 2 Na-pyruvate, and 5 Na-Hepes. Hair bundles instead projected into an artificial endolymph of composition (in mM): 2 NaCl, 118 KCl, 0.25 $CaCl_2$, 3 D-glucose, and 5 Na-Hepes. To disconnect the hair bundles from the overlying otolithic membrane, the apical surface of the preparation was exposed for 20–30 min to endolymph supplemented with 50–67 mg·mL^{-1} of the protease subtilisin (type XXIV or VIII, Sigma). The otolithic membrane was then peeled off to obtain access to individual hair bundles. Experiments were performed at room temperature.

Microscopic Apparatus and Mechanical Stimulation. The preparation was viewed through a 60× water-immersion objective of an upright microscope (BX51WI, Olympus). The tip of a stimulus fiber was affixed to the kinociliary bulb of an individual hair bundle and imaged at a magnification of 1000× onto a displacement monitor that included a dual photodiode. Calibration was performed by measuring the output voltages of the monitor in response to a series of offset displacements of the photodiode. For movements of the fiber's tip that did not exceed ±150 nm in the sample plane, the displacement monitor was linear. Stimulus fibers were fabricated from borosilicate capillaries and coated with a thin layer of gold-palladium to enhance contrast.

The fiber was secured by its base to a stack-type piezoelectric actuator (PA-8/14, Piezosystem Jena) driven by a custom-made power supply (Elbatech). The voltage command to the actuator was a symmetric triangle wave that imposed back-and-forth movements of the fiber's base with a peak-to-peak magnitude of 600 nm. Except during the ∼1 ms that it took to reverse the directionality of motion at the end of each half-cycle, the absolute velocity of the base was nearly fixed (*SI Appendix*, Fig. S2). In a typical run, this velocity was increased sequentially from 1 to 300 μm·s^{-1} in nine steps. The fundamental frequency of the stimulus thus varied from 0.8 to 250 Hz, corresponding to a period of stimulation that decreased from 1.2 s to 4 ms. The slowest stimulus was maintained for four cycles. At higher frequencies, the stimulus lasted 2.4 s, corresponding to tens-to-hundreds of cycles of stimulation at each frequency. Because piezoelectric actuators display hysteresis, their movements do not precisely reflect the command signal. The actual movement of the fiber's base was thus recorded with the displacement monitor at a magnification of 294×; the measurement was performed before or after hair-bundle stimulation. Base and tip positions of the fiber were thus measured with the same acquisition line, which ensured that no delay was artificially introduced between the two positions by the recording procedure. Any delay would be erroneously interpreted as friction in our estimates of the external force applied to the hair bundle by the fiber.

Fiber Calibration and Force Determination. We characterized the mechanical properties of a fiber immersed in endolymph by analyzing the Brownian motion of the free fiber's tip while the base was clamped at a fixed position (*SI Appendix*, section 2.3). The power spectrum of fluctuations was fitted by a Lorentzian, which provided a stiffness k = 200–500 μN·m^{-1} and a drag coefficient λ = 80–140 nN·s·m^{-1}. As far as fluctuations were concerned, the fiber thus behaved as a first-order low-pass filter with an angular cutoff frequency $\omega_1 = k/\lambda = 1.5 - 5.5 \times 10^3$ rad·s^{-1}.

For each triangle wave of stimulation, we computed the mean cycle of the fiber's tip $X(t)$ and base $\Delta(t)$ positions as a function of time t by performing ensemble averages over all cycles of the corresponding waveforms. We then computed the first 30 Fourier components of the average cycles. For the fiber's base, they are given by $\tilde{\Delta}_n = (2/T) \int_0^T \Delta(t)\, e^{+i\, n\, \omega_0\, t} dt$ for $1 \leq n \leq 30$ and $\tilde{\Delta}_0 = \langle \Delta(t) \rangle$ where $T = 2\pi/\omega_0$ is the period of the stimulus and $i^2 = -1$. Similar relations can be written for the Fourier components $\tilde{X}_n$ of tip motion. Assuming that the stimulus fiber behaves as a slender rod, the force applied by the fiber's tip on the hair bundle was then calculated as (*SI Appendix*, section 2)

$$F(t) = \mathrm{Re}\left(\sum_{n=0}^{30} \left[\tilde{F}_n\, e^{-i\, n\, \omega_0\, t} \right] \right), \qquad [3]$$

in which the n^{th} Fourier component of the force is given by

$$\tilde{F}_n = \frac{4}{\beta_1^4} k\ \alpha_n^3 \left[\frac{1 + \cos\alpha_n \times \cosh\alpha_n}{\cos\alpha_n \times \sinh\alpha_n - \sin\alpha_n \times \cosh\alpha_n} \tilde{X}_n - \frac{\cos\alpha_n + \cosh\alpha_n}{\cos\alpha_n \times \sinh\alpha_n - \sin\alpha_n \times \cosh\alpha_n} \tilde{\Delta}_n \right]. \qquad [4]$$

Here we introduced the frequency-dependent parameter $\alpha_n^4 = i\, n\, \omega_0/\omega_S$, with $\omega_S = \omega_1/\beta_1^4$, ω_1 the angular cutoff frequency of thermal fluctuations of the fiber's tip (see previous paragraph), and in which $\beta_1 \cong 1.8751$ is the smallest positive solution of $\cos\beta_1 \times \cosh\beta_1 = -1$. Data analysis was performed with Matlab (the Mathworks, version R2011b).

Iontophoresis of a Channel Blocker and of a Ca^{2+} Chelator. We used iontophoresis of gentamicin to reversibly block the transduction channels of a hair bundle (12). With the same technique, we also applied the chelator 1,2-bis(2-aminophenoxy)ethane-N,N,N′,N′-tetraacetic acid (BAPTA) to sever the tip links by locally reducing the endolymphatic Ca^{2+} concentration. Coarse microelectrodes were fabricated from borosilicate capillaries with a pipette

puller (P97, Sutter Instrument). The resistance of the electrodes was 10 MΩ when filled with 3 M KCl and immersed in the same solution. For the experiments the electrodes were filled with 500 mM gentamicin sulfate (G-4793, Sigma) or with 500 mM BAPTA (A4926, Sigma). These compounds were each dissolved in an aqueous solution containing 25 mM KCl. In each experiment, the electrode's tip was situated at ~3 μm from the hair bundle. Under control conditions, a holding current was applied to counteract the diffusive release of ions from the electrode.

Signal Generation and Acquisition. All signals were generated and acquired under the control of a computer running a user interface programmed with LabVIEW software (version 2011; National Instruments). The command signal controlling the movement of the base of a stimulus fiber was produced by a 16-bit interface card at a sampling rate of 25 kHz (PCI-6733, National Instruments). A second interface card (PCI-6250, National Instruments) conducted signal acquisition with a precision of 16 bits and a sampling rate of 25 kHz. Signals coming from the displacement monitor or going to the stimulation apparatus were conditioned with an eight-pole Bessel antialiasing filter adjusted to a low-pass half-power frequency of 12.5 and 0.5 kHz, respectively.

ACKNOWLEDGMENTS. We thank Jonathon Howard, Thomas Risler, Erik Schäffer, and Mélanie Tobin for comments on the manuscript, and Benoît Lemaire and Rémy Fert from the machine shop of the Curie Institute. This work was supported by the French National Agency for Research (ANR-11-BSV5-0011). V.B. was supported by a long-term fellowship of the Federation of European Biochemical Societies. J.B. is alumnus of the Frontiers in Life Science PhD program of the University Paris Diderot and thanks the Fondation Pierre-Gilles de Gennes for a doctoral fellowship.

1. Gillespie PG, Müller U (2009) Mechanotransduction by hair cells: Models, molecules, and mechanisms. *Cell* 139(1):33–44.
2. Kozlov AS, Baumgart J, Risler T, Versteegh CP, Hudspeth AJ (2011) Forces between clustered stereocilia minimize friction in the ear on a subnanometre scale. *Nature* 474(7351):376–379.
3. Denk W, Webb WW, Hudspeth AJ (1989) Mechanical properties of sensory hair bundles are reflected in their Brownian motion measured with a laser differential interferometer. *Proc Natl Acad Sci USA* 86(14):5371–5375.
4. Kozlov AS, Andor-Ardó D, Hudspeth AJ (2012) Anomalous Brownian motion discloses viscoelasticity in the ear's mechanoelectrical-transduction apparatus. *Proc Natl Acad Sci USA* 109(8):2896–2901.
5. Nadrowski B, Martin P, Jülicher F (2004) Active hair-bundle motility harnesses noise to operate near an optimum of mechanosensitivity. *Proc Natl Acad Sci USA* 101(33): 12195–12200.
6. Hudspeth AJ (2008) Making an effort to listen: mechanical amplification in the ear. *Neuron* 59(4):530–545.
7. Ashmore J, et al. (2010) The remarkable cochlear amplifier. *Hear Res* 266(1–2):1–17.
8. Fettiplace R, Hackney CM (2006) The sensory and motor roles of auditory hair cells. *Nat Rev Neurosci* 7(1):19–29.
9. Barral J, Martin P (2011) The physical basis of active mechanosensitivity by the hair-cell bundle. *Curr Opin Otolaryngol Head Neck Surg* 19(5):369–375.
10. Barral J, Dierkes K, Lindner B, Jülicher F, Martin P (2010) Coupling a sensory hair-cell bundle to cyber clones enhances nonlinear amplification. *Proc Natl Acad Sci USA* 107(18):8079–8084.
11. Gummer AW, Hemmert W, Zenner HP (1996) Resonant tectorial membrane motion in the inner ear: its crucial role in frequency tuning. *Proc Natl Acad Sci USA* 93(16): 8727–8732.
12. Martin P, Bozovic D, Choe Y, Hudspeth AJ (2003) Spontaneous oscillation by hair bundles of the bullfrog's sacculus. *J Neurosci* 23(11):4533–4548.
13. Howard J, Hudspeth AJ (1988) Compliance of the hair bundle associated with gating of mechanoelectrical transduction channels in the bullfrog's saccular hair cell. *Neuron* 1(3):189–199.
14. Martin P, Hudspeth AJ (1999) Active hair-bundle movements can amplify a hair cell's response to oscillatory mechanical stimuli. *Proc Natl Acad Sci USA* 96(25):14306–14311.
15. Corey DP, Hudspeth AJ (1983) Kinetics of the receptor current in bullfrog saccular hair cells. *J Neurosci* 3(5):962–976.
16. Tawada K, Sekimoto K (1991) Protein friction exerted by motor enzymes through a weak-binding interaction. *J Theor Biol* 150(2):193–200.
17. Tinevez JY, Jülicher F, Martin P (2007) Unifying the various incarnations of active hair-bundle motility by the vertebrate hair cell. *Biophys J* 93(11):4053–4067.
18. Kozlov AS, Risler T, Hinterwirth AJ, Hudspeth AJ (2012) Relative stereociliary motion in a hair bundle opposes amplification at distortion frequencies. *J Physiol* 590(Pt 2): 301–308.
19. Holton T, Hudspeth AJ (1986) The transduction channel of hair cells from the bull-frog characterized by noise analysis. *J Physiol* 375(1):195–227.
20. Beurg M, Fettiplace R, Nam JH, Ricci AJ (2009) Localization of inner hair cell mechanotransducer channels using high-speed calcium imaging. *Nat Neurosci* 12(5):553–558.
21. de Gennes P-G (1979) *Scaling Concepts In Polymer Physics*. (Cornell Univ Press, Ithaca), pp 170, 198.
22. Ansari A, Jones CM, Henry ER, Hofrichter J, Eaton WA (1992) The role of solvent viscosity in the dynamics of protein conformational changes. *Science* 256(5065): 1796–1798.
23. Evans E (2001) Probing the relation between force—lifetime—and chemistry in single molecular bonds. *Annu Rev Biophys Biomol Struct* 30:105–128.
24. Braun M, et al. (2011) Adaptive braking by Ase1 prevents overlapping microtubules from sliding completely apart. *Nat Cell Biol* 13(10):1259–1264.
25. Evans EA, Calderwood DA (2007) Forces and bond dynamics in cell adhesion. *Science* 316(5828):1148–1153.
26. Bormuth V, Varga V, Howard J, Schäffer E (2009) Protein friction limits diffusive and directed movements of kinesin motors on microtubules. *Science* 325(5942):870–873.
27. van Netten SM, Kros CJ (2000) Gating energies and forces of the mammalian hair cell transducer channel and related hair bundle mechanics. *Proc Biol Sci* 267(1455): 1915–1923.
28. Markin VS, Hudspeth AJ (1995) Gating-spring models of mechanoelectrical transduction by hair cells of the internal ear. *Annu Rev Biophys Biomol Struct* 24:59–83.
29. Martin P, Mehta AD, Hudspeth AJ (2000) Negative hair-bundle stiffness betrays a mechanism for mechanical amplification by the hair cell. *Proc Natl Acad Sci USA* 97(22):12026–12031.
30. Martin P, Hudspeth AJ, Jülicher F (2001) Comparison of a hair bundle's spontaneous oscillations with its response to mechanical stimulation reveals the underlying active process. *Proc Natl Acad Sci USA* 98(25):14380–14385.
31. Nam JH, Fettiplace R (2008) Theoretical conditions for high-frequency hair-bundle oscillations in auditory hair cells. *Biophys J* 95(10):4948–4962.
32. Fettiplace R, Fuchs PA (1999) Mechanisms of hair cell tuning. *Annu Rev Physiol* 61: 809–834.
33. Martin P (2008) *Active Hair-Bundle Motility of the Hair Cells of Vestibular and Auditory Organs. Active Processes and Otoacoustic Emissions in Hearing, Springer Handbook of Auditory Research*, eds Manley GA, Popper AN, Fay RR (Springer, New York), pp 93–143.
34. Martin P, Hudspeth AJ (2001) Compressive nonlinearity in the hair bundle's active response to mechanical stimulation. *Proc Natl Acad Sci USA* 98(25):14386–14391.
35. Camalet S, Duke T, Jülicher F, Prost J (2000) Auditory sensitivity provided by self-tuned critical oscillations of hair cells. *Proc Natl Acad Sci USA* 97(7):3183–3188.
36. Duke T, Jülicher F (2008) *Critical Oscillators as Active Elements in Hearing. Active Processes and Otoacoustic Emissions, Springer Handbook of Auditory Research*, eds Manley GA, Popper AN, Fay RR (Springer, New York), pp 63–92.
37. Ricci AJ, Kennedy HJ, Crawford AC, Fettiplace R (2005) The transduction channel filter in auditory hair cells. *J Neurosci* 25(34):7831–7839.
38. Ricci A (2002) Differences in mechano-transducer channel kinetics underlie tonotopic distribution of fast adaptation in auditory hair cells. *J Neurophysiol* 87(4):1738–1748.
39. Lim DJ (1986) Functional structure of the organ of Corti: A review. *Hear Res* 22(1-3): 117–146.
40. Roth B, Bruns V (1992) Postnatal development of the rat organ of Corti. II. Hair cell receptors and their supporting elements. *Anat Embryol (Berl)* 185(6):571–581.
41. Kennedy HJ, Evans MG, Crawford AC, Fettiplace R (2003) Fast adaptation of mechanoelectrical transducer channels in mammalian cochlear hair cells. *Nat Neurosci* 6(8): 832–836.